2011

Can water vapour process data be used to estimate precipitation efficiency?

Shouting Gao
Chinese Academy of Sciences, gst@lasg.iap.ac.cn

Xiaofan Li
NOAA/NESDIS/Center for Satellite Applications and Research

RMetS
Royal Meteorological Society

Can water vapour process data be used to estimate precipitation efficiency?

Shouting Gao[a]* and Xiaofan Li[b]†

[a]*Laboratory of Cloud-Precipitation Physics and Severe Storms, Institute of Atmospheric Physics, Chinese Academy of Sciences, Beijing, China*

[b]*NOAA/NESDIS/Center for Satellite Applications and Research, Camp Springs, Maryland, USA*

*Correspondence to: S. Gao, Institute of Atmospheric Physics, CAS, Beijing 100029, China. E-mail: gst@lasg.iap.ac.cn

†The contribution of X. Li to this article was prepared as part of his official duties as a US Federal Government employee.

The precipitation efficiencies (*RMPE, CMPE*, and *LSPE*) can be defined as the ratio of rain rate to rainfall sources in the rain microphysical budget, the cloud microphysical budget, and the surface rainfall budget, respectively. The estimate of *RMPE* from grid-scale data serves as the true precipitation efficiency since the rain rate is a diagnostic term in the tropical rain microphysical budget. The accuracy of precipitation efficiency estimates with *CMPE* and *LSPE* is compared to that of *RMPE* by analyzing data from a 21-day two-dimensional cloud-resolving model simulation with imposed large-scale vertical velocity, zonal wind, and horizontal advection obtained from the Tropical Ocean Global Atmosphere Coupled Ocean–Atmosphere Response Experiment. The results show *CMPE* is generally smaller than *RMPE*. The root-mean-squared difference between *RMPE* and *LSPE* is larger than the standard deviation of *RMPE*. Thus, water vapour process data cannot be used to estimate precipitation efficiency. Copyright © 2011 Royal Meteorological Society

Key Words: rainfall source; cloud-resolving model

Received 1 September 2010; Revised 1 February 2011; Accepted 9 February 2011; Published online in Wiley Online Library 3 May 2011

Citation: Gao S, Li X. 2011. Can water vapour process data be used to estimate precipitation efficiency?. *Q. J. R. Meteorol. Soc.* **137**: 969–978. DOI:10.1002/qj.806

1. Introduction

Precipitation efficiency is an important physical parameter in convective systems and has been applied to determine the rainfall intensity in operational precipitation forecasts (e.g. Doswell *et al.*, 1996). Since Braham (1952) calculated precipitation efficiency with the inflow of water vapour into the storm through cloud base as the rainfall source more than half century ago, precipitation efficiency has been defined as the ratio of the precipitation rate to the sum of all precipitation sources. This definition of large-scale precipitation efficiency (*LSPE*) has been modified and widely applied in modelling studies and operational forecasts (e.g. Auer and Marwitz, 1968; Heymsfield and Schotz, 1985; Chong and Hauser, 1989; Doswell *et al.*, 1996; Ferrier *et al.*, 1996; Li *et al.* 2002; Tao *et al.*, 2004; Sui *et al.*, 2005). Due to the fact that prognostic cloud microphysical parametrization schemes are used in cloud-resolving modelling of convective processes, precipitation efficiency is also defined through cloud microphysical budgets as cloud microphysics precipitation efficiency (*CMPE*; e.g. Weisman and Klemp, 1982; Lipps and Hemler, 1986; Ferrier *et al.*, 1996; Li *et al.*, 2002; Sui *et al.*, 2005). While estimates of *CMPE* and *LSPE* can be more than 100% and *LSPE* estimates can be negative, they are altered to fall within the normal range of 0–100% through the inclusion of all rainfall sources and the exclusion of all rainfall sinks from the surface rainfall budget for *LSPE* (Gao *et al.*, 2005), and the cloud microphysical budget for *CMPE* (Sui *et al.*, 2007).

While the precipitation efficiencies in the previous studies have been defined in the surface rainfall budget derived from water vapour and cloud budgets and in the cloud microphysical budget derived from the microphysical

budgets of five cloud species (cloud water, rain, cloud ice, snow, and graupel; e.g. Li *et al.*, 2002; Sui *et al.*, 2007), we argue that the precipitation efficiency can be defined only in the budget where precipitation rate is a diagnostic term. An example of such a primitive budget is the rain microphysical budget in the Tropics. Thus, the rain microphysical budget is used to define rain microphysics precipitation efficiency (*RMPE*) and its estimate from grid-scale simulation data serves as the 'true' precipitation efficiency in this study. *LSPE* and *CMPE* may deviate from *RMPE* because only rainfall sources are used to estimate precipitation efficiency. Do *CMPE* and *LSPE* deviate from *RMPE*? What causes the differences? Can water vapour process data be used to estimate precipitation efficiency? These questions will be discussed by analyzing a 21-day two-dimensional (2D) cloud-resolving model simulation that is forced by the large-scale forcing derived from the Tropical Ocean Global Atmosphere Coupled Ocean–Atmosphere Response Experiment (TOGA COARE). In the next section, the cloud model, forcing, and experiment are described. The results are presented in section 3. The summary is given in section 4.

2. Model and experiment

The cloud-resolving model used in this study is the 2D version of the Goddard Cumulus Ensemble Model, which was originally developed by Soong and Ogura (1980), Soong and Tao (1980), and Tao and Simpson (1993) and was modified by Li *et al.* (1999). The model has prognostic equations of potential temperature, specific humidity, mixing ratios of cloud water, raindrop, cloud ice, snow, and graupel, and perturbation momentum. The model also includes the cloud microphysical parametrization schemes (Lin *et al.*, 1983; Rutledge and Hobbs, 1983, 1984; Tao *et al.*, 1989; Krueger *et al.*, 1995) and interactive solar and thermal infrared radiation parametrization schemes (Chou *et al.*, 1991, 1998; Chou and Suarez, 1994). The model uses cyclic lateral boundaries, a horizontal domain of 768 km, a horizontal grid resolution of 1.5 km, 33 vertical levels, and a time step of 12 s. Detailed model descriptions can be found in Gao and Li (2008).

The model is forced by zonally uniform vertical velocity, zonal wind, and thermal and moisture advection based on 6-hourly TOGA COARE observations within the Intensive Flux Array (IFA) region (Zhang, personal communication, 1999). The calculations are based on a constrained, variational method applied to column-integrated budgets of mass, heat, moisture, and momentum as proposed by Zhang and Lin (1997). Hourly sea surface temperature (SST) at the Improved Meteorological (IMET) surface mooring buoy (1.75°S, 156°E) (Weller and Anderson, 1996) is also imposed in the model. The model is integrated from 0400 LST on 18 December 1992 to 1000 LST on 9 January 1993 (a total of 486 h). Figure 1 shows the time evolution of the vertical distribution of the large-scale vertical velocity and zonal wind and the time series of the SST, which are imposed in the model during the integrations. The 21-day simulation data have been applied to the analysis of precipitation processes including the roles of surface evaporation (Cui and Li, 2006), ice microphysics (Gao *et al.*, 2006), precipitation efficiency (Li *et al.*, 2002; Sui *et al.*, 2005, 2007), and diurnal variation (Gao *et al.*, 2009). Hourly simulation data are used in this study.

3. Results

3.1. RMPE: 'true' precipitation efficiency

The mass-integrated rain microphysical budget in the Tropics is used to define *RMPE*, which can be written as

$$P_S - Q_{RM} = \sum_{I=1}^{12} RP_I, \tag{1}$$

where

$$P_S = \overline{\rho} w_{Tr} q_r |_{z=0}, \tag{1a}$$

$$Q_{RM} = -\frac{\partial [q_r]}{\partial t} - \left[u \frac{\partial q_r}{\partial x} \right] - \left[w \frac{\partial q_r}{\partial z} \right], \tag{1b}$$

$$\begin{aligned} RP_I = \{ & [P_{SACW}(T > T_0)], [P_{RAUT}], [P_{RACW}], \\ & [P_{GACW}(T > T_0)], -[P_{REVP}], [P_{RACS}(T > T_0)], \\ & -[P_{IACR}(T < T_0)], -[P_{GACR}(T < T_0)], \\ & -[P_{SACR}(T < T_0)], -[P_{GFR}(T < T_0)], \\ & [P_{SMLT}(T > T_0)], [P_{GMLT}(T > T_0)] \}. \end{aligned} \tag{1c}$$

Here, P_S is surface rain rate; $\overline{\rho}$ is air density, which is height dependent only; w_{Tr} is terminal velocity for rain, q_r is the mixing ratio of rain; z is vertical coordinate; u and w are the zonal and vertical components of wind, respectively; RP_I denotes the rainfall source/sink terms from rain microphysical processes, which are defined in Table I, and $T_0 = 0°C$. $[(\dots)] = \int_{z_b}^{z_t} \overline{\rho}(\dots) dz$, where z_t and z_b are the heights of the top and bottom of the model atmosphere respectively.

Thus, *RMPE* is defined as

$$RMPE = \frac{P_S}{RSRB}, \tag{2}$$

where $RSRB$ $(= RSR + H(Q_{RM})Q_{RM})$ is the rainfall source from rain microphysical budget;

RSR $\left(= \sum_{I=1}^{12} H(RP_I) RP_I \right)$ is the rainfall source from rain microphysical processes, and

H is the Heaviside function,

$$H(F) = \begin{cases} 1 \text{ if } F > 0, \\ 0 \text{ if } F \le 0. \end{cases}$$

RMPE is calculated using hourly data and accumulating rainfall sources (*RSRB*) from each model grid over the model domain, which serves as the 'true' precipitation efficiency.

3.2. CMPE versus RMPE

Sui *et al.* (2007) used the cloud microphysical budget to define precipitation efficiency (*CMPE*). The cloud microphysical budget can be expressed by

$$P_s - Q_{CM} = \sum_{I=1}^{7} P_I, \tag{3}$$

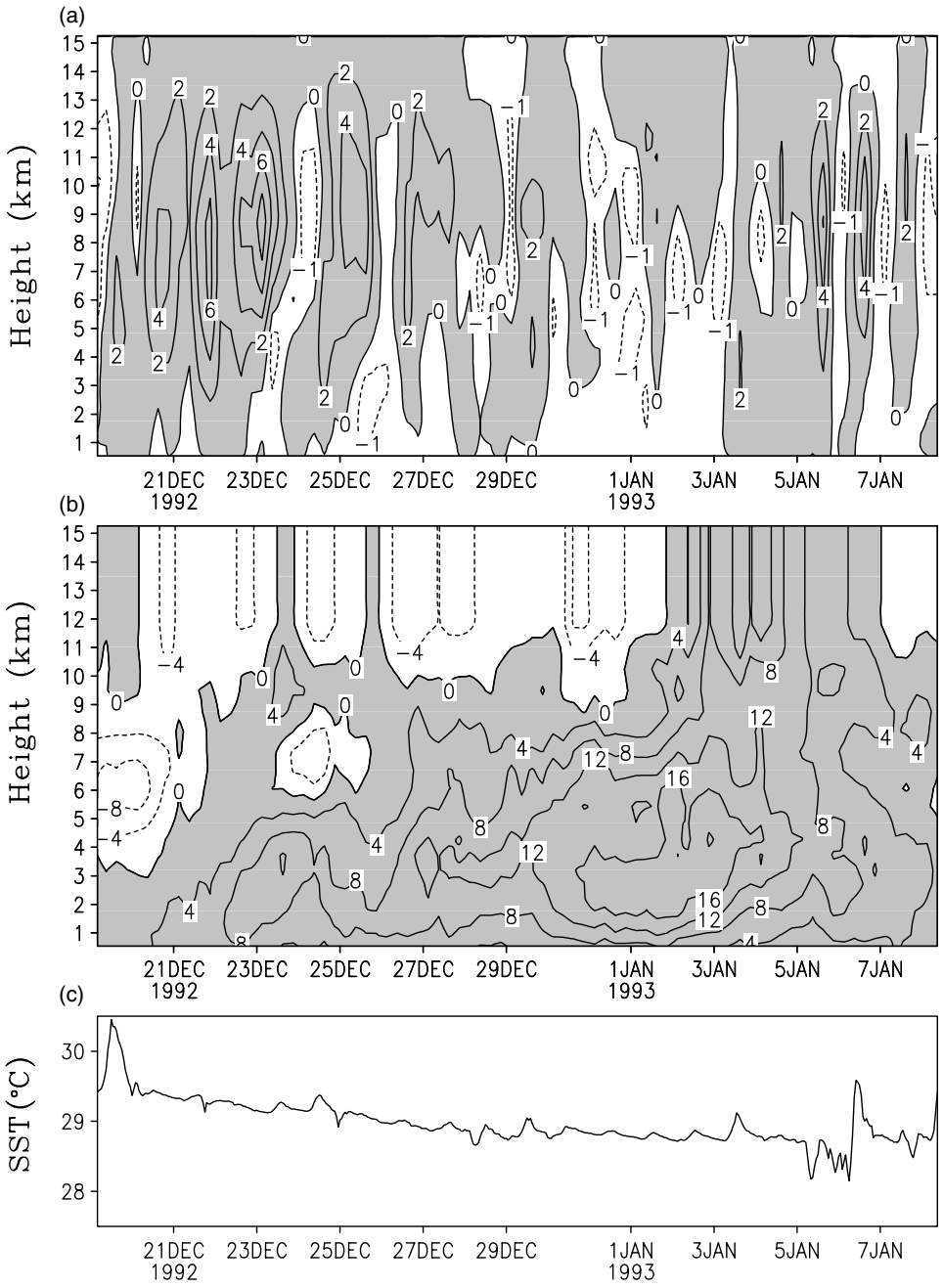

Figure 1. Time – height cross-sections of (a) vertical velocity (cm s^{-1}), and (b) zonal wind speed (m s^{-1}), and time series of (c) sea surface temperature (°C) observed and derived from TOGA COARE for the 21-day period. Upward motion in (a) and westerly winds in (b) are shaded.

where

$$P_S = \overline{\rho} w_{Tr} q_r |_{z=0}, \tag{3a}$$

$$Q_{CM} = -\frac{\partial [q_l]}{\partial t} - \left[\frac{\partial q_l}{\partial x}\right] - \left[\frac{\partial q_l}{\partial z}\right], \tag{3b}$$

$$P_I = ([P_{CND}], [P_{DEP}], [P_{SDEP}], [P_{GDEP}], -[P_{REVP}], -[P_{MLTG}], -[P_{MLTS}]). \tag{3c}$$

Here, $q_l = q_c + q_r + q_i + q_s + q_g$, where q_c, q_r, q_i, q_s, q_g are the mixing ratios of cloud water, raindrops, cloud ice, snow, and graupel, respectively; P_I denotes rainfall source/sink terms from cloud microphysical processes, which are defined in Table I. Thus, *CMPE* is defined as

$$CMPE = \frac{P_S}{RSC + H(Q_{CM}) Q_{CM}}, \tag{4}$$

where $RSC \left(= \sum_{I=1}^{7} H(P_I) P_I\right)$ is the rainfall source from cloud microphysical processes.

Rainfall sources are used to calculate precipitation efficiency, whereas rainfall sinks are excluded, which can yield the difference between *RMPE* and *CMPE*. This is demonstrated in Figure 2 where *RMPE* is larger than *CMPE*. *RMPE* and *CMPE* are calculated by accumulating rainfall sources from each model grid over the model domain in Figure 2.

Since the cloud microphysical budget is derived by combining mass-integrated microphysical budgets of cloud water, rain, cloud ice, snow, and graupel, the difference between *RMPE* and *CMPE* can be contributed to by microphysical budgets of cloud water, cloud ice, snow,

Table I. List of microphysical processes and their parametrization schemes.

Notation	Growth of:	By:	Scheme*
P_{MLTG}	Vapour	Evaporation of liquid from graupel surface	RH84
P_{MLTS}	Vapour	Evaporation of melting snow	RH83
P_{REVP}	Vapour	Evaporation of raindrops	RH83
P_{IMLT}	Cloud water	Melting of cloud ice	RH83
P_{CND}	Cloud water	Condensation of supersaturated vapour	TSM
P_{GMLT}	Raindrops	Melting of graupel	RH84
P_{SMLT}	Raindrops	Melting of snow	RH83
P_{RACI}	Raindrops	Accretion of cloud ice	RH84
P_{RACW}	Raindrops	Collection of cloud water	RH83
P_{RACS}	Raindrops	Accretion of snow	RH84
P_{RAUT}	Raindrops	Autoconversion of cloud water	LFO
P_{IDW}	Cloud ice	Deposition of cloud water	KFLC
P_{IACR}	Cloud ice	Accretion of rain	RH84
P_{IHOM}	Cloud ice	Homogeneous freezing of cloud water	
P_{DEP}	Cloud ice	Deposition of supersaturated vapour	TSM
P_{SAUT}	Snow	Conversion of cloud ice	RH83
P_{SACI}	Snow	Collection of cloud ice	RH83
P_{SACW}	Snow	Accretion of cloud water	RH83
P_{SFW}	Snow	Deposition of cloud water	KFLC
P_{SFI}	Snow	Deposition from cloud ice	KFLC
P_{SACR}	Snow	Accretion of raindrops	LFO
P_{SDEP}	Snow	Deposition of vapour	RH83
P_{GACI}	Graupel	Collection of cloud ice	RH84
P_{GACR}	Graupel	Accretion of raindrops	RH84
P_{GACS}	Graupel	Accretion of snow	RH84
P_{GACW}	Graupel	Accretion of cloud water	RH84
P_{WACS}	Graupel	Riming of snow	RH84
P_{GDEP}	Graupel	Deposition of vapour	RH84
P_{GFR}	Graupel	Freezing of raindrops	LFO

*KFLC: Krueger *et al.* (1995). LFO: Lin *et al.* (1983).
RH83, RH84: Rutledge and Hobbs (1983,1984). TSM: Tao *et al.* (1989).

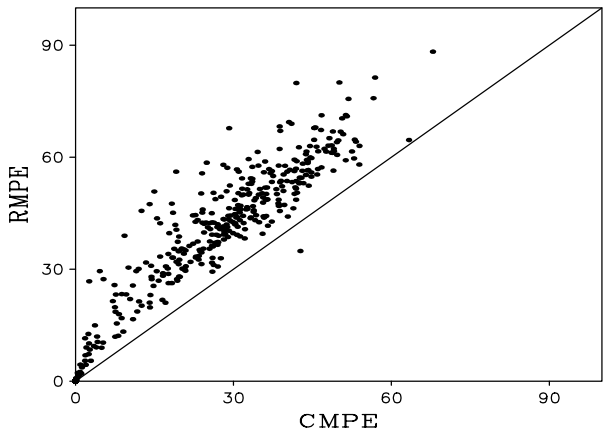

Figure 2. *RMPE* versus *CMPE* (%). *RMPE* and *CMPE* are calculated by using hourly data and accumulating rainfall sources from each model grid over the model domain. The diagonal line denotes *RMPE=CMPE*.

and graupel. The budgets can be written as

$$Q_{\mathrm{CWM}} + \sum_{I=1}^{9} CWP_I = 0, \tag{5a}$$

$$Q_{\mathrm{CIM}} + \sum_{I=1}^{9} CIP_I = 0, \tag{5b}$$

$$Q_{\mathrm{SM}} + \sum_{I=1}^{15} SP_I = 0, \tag{5c}$$

$$Q_{\mathrm{GM}} + \sum_{I=1}^{14} GP_I = 0, \tag{5d}$$

where

$$Q_{\mathrm{CWM}} = -\frac{\partial [q_{\mathrm{c}}]}{\partial t} - \left[u\frac{\partial q_{\mathrm{c}}}{\partial x}\right] - \left[w\frac{\partial q_{\mathrm{c}}}{\partial z}\right], \tag{6a}$$

$$Q_{\mathrm{CIM}} = -\frac{\partial [q_{\mathrm{i}}]}{\partial t} - \left[u\frac{\partial q_{\mathrm{i}}}{\partial x}\right] - \left[w\frac{\partial q_{\mathrm{i}}}{\partial z}\right], \tag{6b}$$

$$Q_{\mathrm{SM}} = -\frac{\partial [q_{\mathrm{s}}]}{\partial t} - \left[u\frac{\partial q_{\mathrm{s}}}{\partial x}\right] - \left[w\frac{\partial q_{\mathrm{s}}}{\partial z}\right], \tag{6c}$$

$$Q_{\mathrm{GM}} = -\frac{\partial [q_{\mathrm{g}}]}{\partial t} - \left[u\frac{\partial q_{\mathrm{g}}}{\partial x}\right] - \left[\frac{\partial q_{\mathrm{g}}}{\partial z}\right], \tag{6d}$$

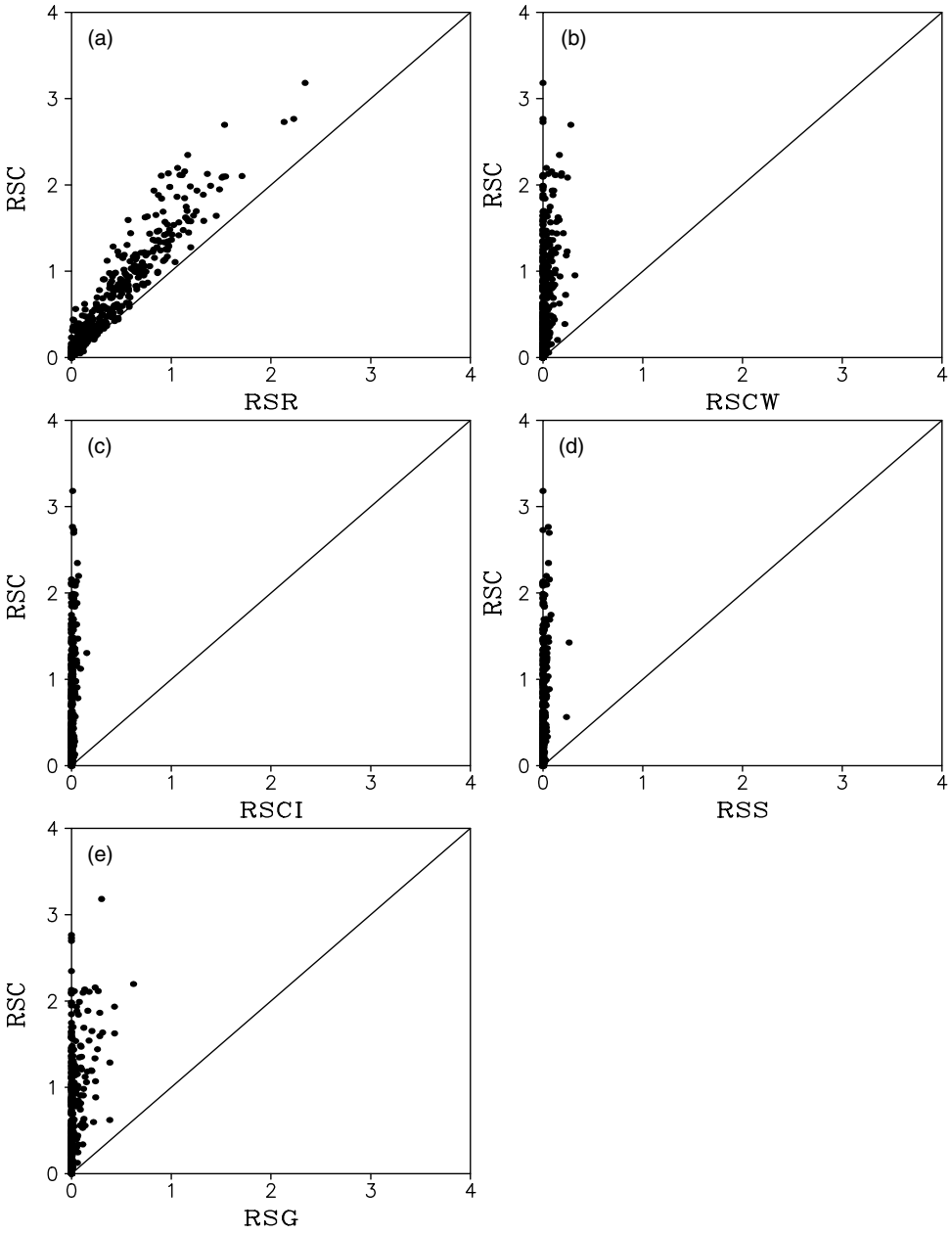

Figure 3. (a) Rainfall source from cloud microphysics (*RSC*) versus rainfall source from rain microphysics (*RSR*), (b) *RSC* versus rainfall source from cloud water microphysics (*RSCW*), (c) *RSC* versus rainfall source from cloud ice microphysics (*RSCI*), (d) *RSC* versus rainfall source from snow microphysics (*RSS*), and (e) RSC versus rainfall source from graupel microphysics (*RSG*). Calculations are conducted by accumulating rainfall sources from each model grid over the model domain. The diagonal lines denote 1:1 equivalences.

$$CWP_I = \{-P_{\mathrm{SACW}}, -P_{\mathrm{RAUT}}, -P_{\mathrm{RACW}}, -P_{\mathrm{SFW}}(T < T_0), -P_{\mathrm{GACW}}, P_{CND}, -P_{\mathrm{IHOM}}(T < T_{00}), P_{\mathrm{IMLT}}(T > T_0), -P_{\mathrm{IDW}}(T_{00} < T < T_0)\}, \quad (6e)$$

$$CIP_I = -P_{\mathrm{SAUT}}(T < T_0), -P_{\mathrm{SACI}}(T < T_0), -P_{\mathrm{RACI}}(T < T_0), -P_{\mathrm{SFI}}(T < T_0), -P_{\mathrm{GACI}}(T < T_0), P_{\mathrm{IHOM}}(T < T_{00}), -P_{\mathrm{IMLT}}(T > T_0), P_{\mathrm{IDW}}(T_{00} < T < T_0), P_{\mathrm{DEP}}\}, \quad (6f)$$

$$SP_I = \{P_{\mathrm{SAUT}}(T < T_0), P_{\mathrm{SACI}}(T < T_0), P_{\mathrm{SACW}}(T < T_0), P_{\mathrm{SFW}}(T < T_0), P_{\mathrm{SFI}}(T < T_0), P_{\mathrm{RACI}}(T < T_0), -P_{\mathrm{RACS}}(T > T_0), -P_{\mathrm{GACS}}, -P_{\mathrm{SMLT}}(T > T_0), -P_{\mathrm{RACS}}(T < T_0), P_{\mathrm{SACR}}(T < T_0), P_{\mathrm{SDEP}}(T < T_0), -P_{\mathrm{MLTS}}(T > T_0), P_{\mathrm{IACR}}(T < T_0), -P_{\mathrm{WACS}}(T < T_0)\}, \quad (6g)$$

$$GP_I = \{P_{\mathrm{RACI}}(T < T_0), P_{\mathrm{GACI}}(T < T_0), P_{\mathrm{GACW}}(T < T_0), P_{\mathrm{SACW}}(T < T_0), P_{\mathrm{GACS}}, P_{\mathrm{IACR}}(T < T_0), P_{\mathrm{GACR}}(T < T_0),$$

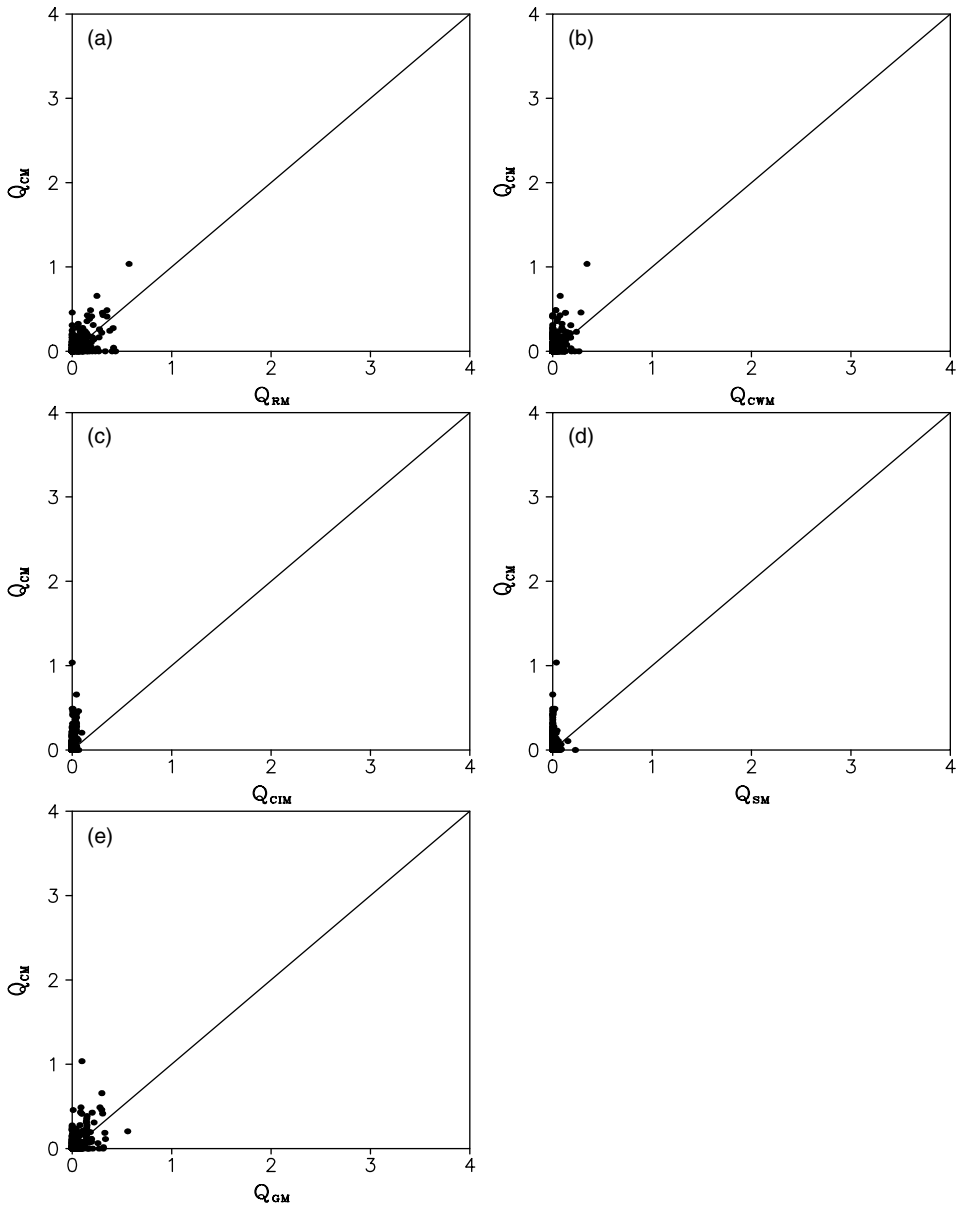

Figure 4. (a) $H(Q_{CM})Q_{CM}$ versus $H(Q_{RM})Q_{RM}$, (b) $H(Q_{CM})Q_{CM}$ versus $H(Q_{CWM})Q_{CWM}$, (c) $H(Q_{CM})Q_{CM}$ versus $H(Q_{CIM})Q_{CIM}$, (d) $H(Q_{CM})Q_{CM}$ versus $H(Q_{SM})Q_{SM}$, and (e) $H(Q_{CM})Q_{CM}$ versus $H(Q_{GM})Q_{GM}$. Calculations are conducted by accumulating each term from each model grid over the model domain. The diagonal lines denote 1:1 equivalences.

$$P_{\mathrm{RACS}}(T < T_0), P_{\mathrm{GFR}}(T < T_0),$$
$$P_{\mathrm{WACS}}(T < T_0), -P_{\mathrm{GMLT}}(T > T_0),$$
$$P_{\mathrm{GDEP}}(T < T_0), -P_{\mathrm{MLTG}}(T > T_0),$$
$$P_{\mathrm{SACR}}(T < T_0)\}. \tag{6h}$$

CWP_I, CIP_I, SP_I, and GP_I denote rainfall source/sink terms from microphysical processes of cloud water, cloud ice, snow, and graupel, respectively. The microphysical processes in (6e)–(6h) are defined in Table I, and $T_{00} = -35^{\circ}\mathrm{C}$.

Since the rainfall sources are obtained by taking positive values for (5a)–(5d), we may get

$$H(Q_{\mathrm{CWM}})Q_{\mathrm{CWM}} + RSCW \neq 0, \tag{7a}$$

$$H(Q_{\mathrm{CIM}})Q_{\mathrm{CIM}} + RSCI \neq 0, \tag{7b}$$

$$H(Q_{\mathrm{SM}})Q_{\mathrm{SM}} + RSS \neq 0, \tag{7c}$$

$$H(Q_{\mathrm{GM}})Q_{\mathrm{GM}} + RSG \neq 0, \tag{7d}$$

where $RSCW \left(= \sum_{I=1}^{9} H(CWP_I)CWP_I\right)$, $RSCI \left(= \sum_{I=1}^{9} H(CIP_I)CIP_I\right)$, $RSS \left(= \sum_{I=1}^{15} H(SP_I)SP_I\right)$, $RSG \left(= \sum_{I=1}^{14} H(GP_I)GP_I\right)$ are the rainfall sources from cloud water, from cloud ice, from snow and from graupel microphysical processes, respectively.

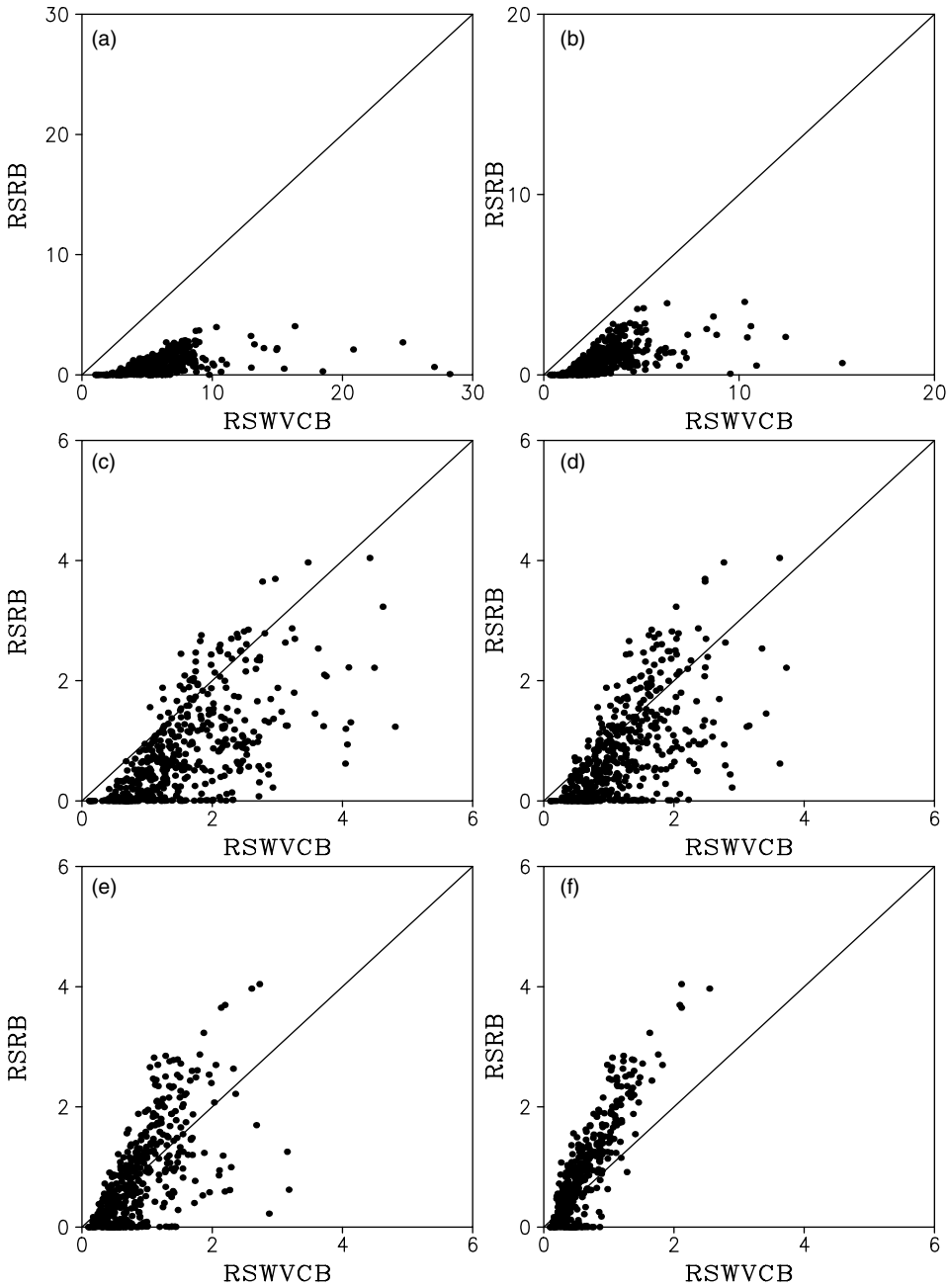

Figure 5. Rainfall source from rain microphysical budget (*RSRB*) versus rainfall source from water vapour and cloud microphysical budget (*RSWVCB*). RSR is calculated by accumulating rainfall sources from each model grid over the model domain with hourly data, whereas *RSWVCB* is calculated by using (a) grid data (1.5 km), (b) 12 km, (c) 96 km, (d) 192 km, (e) 384 km, and (f) 768 km (model domain) mean data. Unit is mm h^{-1}. The diagonal lines denote *RSRB* = *RSWVCB*.

Equations (7a)–(7d) show the possible contributions of microphysical budgets of cloud water, cloud ice, snow, and graupel to the difference between *RMPE* and *CMPE*. This can be demonstrated in Figure 3, which shows *RSC* versus *RSR, RSCW, RSCI, RSS*, and *RSG*, respectively, and in Figure 4, which shows $H(Q_{CM})Q_{CM}$ versus $H(Q_{RM})Q_{RM}$, $H(Q_{CWM})Q_{CWM}$, $H(Q_{CIM})Q_{CIM}$, $H(Q_{SM})Q_{SM}$, and $H(Q_{GM})Q_{GM}$, respectively. The graupel and cloud water microphysical budgets contribute more to the difference in rainfall sources between *RMPE* and *CMPE* than the cloud ice and snow microphysical budgets do, while the cloud microphysical budget (3) is primarily attributable to the rain microphysical budget (1).

3.3. *LSPE versus RMPE*

While cloud information is usually unavailable from conventional data, water vapour processes can be estimated with available conventional data. Sui *et al.* (2007) showed that large-scale precipitation efficiency (*LSPE*) is defined as

$$LSPE = \frac{P_S}{RSWVCB}, \tag{8d}$$

where $RSWVCB \left(= \sum_{I=1}^{4} H(Q_I)Q_I\right)$ is the rainfall source from water vapour and cloud budgets, $Q_I = (Q_{WVT}, Q_{WVF}, Q_{WVE}, Q_{CM})$, where Q_{WVT} is the local vapour change, Q_{WVF} is vapour convergence, and Q_{WVE} is the surface evaporation rate. *LSPE* (8) can be derived from the

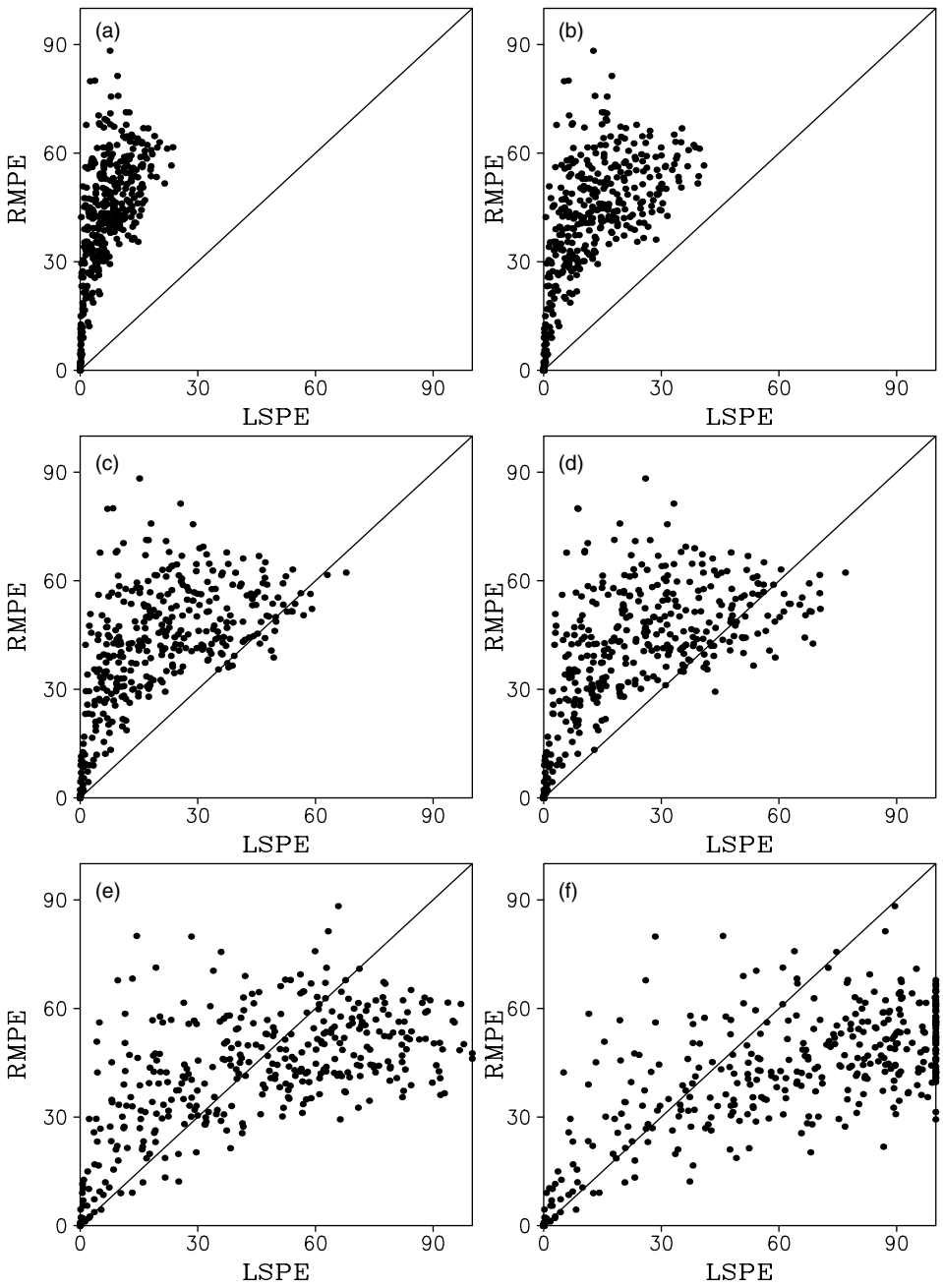

Figure 6. *RMPE* versus *LSPE* (%). *RMPE* is calculated by accumulating rainfall sources from each model grid over the model domain with hourly data, whereas *LSPE* is calculated by using (a) grid data (1.5 km), (b) 12 km, (c) 96 km, (d) 192 km, (e) 384 km, and (f) 768 km (model domain) mean data. The diagonal lines denote *RMPE* = *LSPE*.

surface rainfall budget (Gao *et al.*, 2005; Cui and Li, 2006), which combines the mass-integrated cloud microphysical budget (3) with the mass-integrated water vapour budget, which can be expressed as

$$Q_{\mathrm{WVT}} + Q_{\mathrm{WVF}} + Q_{\mathrm{WVE}} = \sum_{I=1}^{7} P_I = P_{\mathrm{S}} - Q_{\mathrm{CM}}. \qquad (9)$$

The comparison between *RMPE* (2) and *LSPE* (8) indicates that *LSPE*=*RMPE* only when *RSRB* = *RSWVCB*. This is not the case, as indicated in Figure 5. The rainfall source from the rain microphysical budget ($RSRB = RSR + H(Q_{RM})Q_{RM}$) is generally smaller than the rainfall source from the water vapour and cloud microphysical budget $\left(RSWVCB = \sum_{I=1}^{4} H(Q_I)Q_I\right)$ when the water vapour and cloud microphysical budgets are averaged over areas smaller than 192 km (Figures 5(a)–(d)), whereas it is generally larger than *RSWVCB* when the water vapour and cloud microphysical budget is averaged over areas larger than 384 km (Figures 5(e, f)). As a result, *LSPE* is significantly different from *RMPE* (Figure 6). The root-mean-squared (RMS) differences between *RMPE* and *LSPE* are 20.7 to 37.5% (Table II), which are significantly larger than the RMS difference between *RMPE* and *CMPE* (15.3%) and the standard deviation of *RMPE* (18.0%).

Many previous studies showed the effects of vertical wind shear on the development of convective systems and associated rainfall (e.g. Pastushkov, 1975; Corbosiero and Molinari, 2002; Wang *et al.*, 2009; Shen *et al.*, 2011). Vertical wind shear and its standard deviation, σ, is calculated using the vertical zonal-wind difference between 11 km and 3.7 km

Table II. RMS differences between *RMPE* and estimates of *LSPE* using grid-scale (1.5 km) and model-domain mean (768 km) data and data averaged over the areas of 12 km, 96 km, 192 km, and 386 km.

	1.5 km	12 km	96 km	192 km	384 km	768 km
RMS difference (%)	37.5	31.7	23.1	20.7	21.8	31.0

(maximum westerly wind) and categorized wind-shear data into three types: strong shear (wind shear larger than 2σ), moderate shear (wind shear between σ and 2σ), and weak shear (wind shear less than σ). The RMS differences between *LSPE* and *RMPE* are 22.6% for strong shear, 23.3% for moderate shear, and 20.5% for weak shear when *LSPE* is calculated using large-scale data averaged over the area of 384 km. The standard deviations of *RMPE* are 18.2% for strong shear, 17.2% for moderate shear, and 18.1% for weak shear. The RMS differences between RMPE and LSPE are larger than the standard deviations of *RMPE*. The estimate of precipitation efficiency with water vapor process data may not capture the variation of the true precipitation efficiency. Therefore, water vapour process data cannot be used to estimate precipitation efficiency.

4. Summary

In this study, precipitation efficiency (*RMPE*) is first defined through a rain microphysical budget where precipitation rate is a diagnostic term and is considered to be the 'true' precipitation efficiency when it is calculated by accumulating rainfall source from each model grid over the model domain. *RMPE* is then compared with cloud microphysics precipitation efficiency (*CMPE*) defined through a cloud microphysical budget and large-scale precipitation efficiency (*LSPE*) through a water vapour budget. The precipitation efficiencies are calculated using hourly data from a 21-day 2D cloud-resolving model simulation with imposed large-scale vertical velocity, zonal wind and horizontal advection obtained from TOGA COARE data. The calculations with accumulations of rainfall sources from each model grid over the entire model domain show that *CMPE* is generally smaller than *RMPE*. The difference between *RMPE* and *CMPE* is primarily from the graupel and cloud water microphysical budgets. The comparison between *RMPE* and *LSPE* shows that their RMS differences are larger than the standard deviation of *RMPE*. This suggests that water vapour process data may not be used to estimate precipitation efficiency. Since this study only uses 2D simulation data with idealized cyclic lateral boundaries, 3D model simulations are needed to investigate temporal and spatial dependence of precipitation efficiency through analyzing relations between *RMPE, CMPE*, and *LSPE* and to evaluate the calculations of precipitation efficiency with large-scale water vapour process data.

Acknowledgements

The authors thank Prof. M. Zhang (State University of New York at Stony Brook) for his TOGA COARE forcing data, and two anonymous reviewers for their constructive comments. This work is supported by the National Key Basic Research and Development Project of China no. 2009CB421505, and the National Natural Sciences Foundation of China under grant nos. 40930950 and 41075043.

References

Auer AH Jr, Marwitz JD. 1968. Estimates of air and moisture flux into hailstorms on the High Plains. *J. Appl. Meteorol.* **7**: 196–198.

Braham RR Jr. 1952. The water and energy budgets of the thunderstorm and their relation to thunderstorm development. *J. Meteorol.* **9**: 227–242.

Chong M, Hauser D. 1989. A tropical squall line observed during the CORT 81 experiment in West Africa. Part II: Water budget. *Mon. Weather Rev.* **117**: 728–744.

Chou M-D, Suarez MJ. 1994. 'An efficient thermal infrared radiation parameterization for use in general circulation model'. NASA Tech. Memo. 104606, vol. 3. NASA/Goddard Space Flight Center: Greenbelt, MD, USA.

Chou M-D, Kratz DP, Ridgway W. 1991. Infrared radiation parameterization in numerical climate models. *J. Climate* **4**: 424–437.

Chou M-D, Suarez MJ, Ho C-H, Yan MM-H, Lee K-T. 1998. Parameterizations for cloud overlapping and shortwave single scattering properties for use in general circulation and cloud ensemble models. *J. Atmos. Sci.* **55**: 201–214.

Corbosiero KL, Molinari J. 2002. The effects of vertical wind shear on the distribution of convection in tropical cyclones. *Mon. Weather Rev.* **130**: 2110–2123.

Cui X, Li X. 2006. Role of surface evaporation in surface rainfall processes. *J. Geophys. Res.* **111**: D17112, DOI: 10.1029/2005JD006876.

Doswell CA III, Brooks HE, Maddox RA. 1996. Flash flood forecasting: An ingredients-based methodology. *Weather Forecasting* **11**: 560–581.

Ferrier BS, Simpson J, Tao W-K. 1996. Factors responsible for precipitation efficiencies in midlatitude and tropical squall simulations. *Mon. Weather Rev.* **124**: 2100–2125.

Gao S, Li X. 2008. *Cloud-resolving modeling of convective processes*. Springer: Dordrecht, Netherlands.

Gao S, Cui X, Zhu Y, Li X. 2005. Surface rainfall processes as simulated in a cloud-resolving model. *J. Geophys. Res.* **110**: D10202, DOI: 10.1029/2004JD005467.

Gao S, Ran L, Li X. 2006. Impacts of ice microphysics on rainfall and thermodynamic processes in the tropical deep convective regime: A 2D cloud-resolving modeling study. *Mon. Weather Rev.* **134**: 3015–3024.

Gao S, Cui X, Li X. 2009. A modeling study of diurnal rainfall variations during the 21-day period of TOGA COARE. *Adv. Atmos. Sci.* **26**: 895–905.

Heymsfield GM, Schotz S. 1985. Structure and evolution of a severe squall line over Oklahoma. *Mon. Weather Rev.* **113**: 1563–1589.

Krueger SK, Fu Q, Liou KN, Chin H-NS. 1995. Improvement of an ice-phase microphysics parameterization for use in numerical simulations of tropical convection. *J. Appl. Meteorol.* **34**: 281–287.

Li X, Sui C-H, Lau K-M, Chou M-D. 1999. Large-scale forcing and cloud-radiation interaction in the tropical deep convective regime. *J. Atmos. Sci.* **56**: 3028–3042.

Li X, Sui C-H, Lau K-M. 2002. Precipitation efficiency in the tropical deep convective regime: A 2-D cloud resolving modeling study. *J. Meteorol. Soc. Japan*, **80**: 205–212.

Lin Y-L, Farley RD, Orville HD. 1983. Bulk parameterization of the snow field in a cloud model. *J. Climate Appl. Meteorol.* **22**: 1065–1092.

Pastushkov RS. 1975. The effects of vertical wind shear on the evolution of convective clouds. *Q. J. R. Meteorol. Soc.* **101**: 281–291.

Lipps FB, Hemler RS. 1986. Numerical simulation of deep tropical convection associated with large-scale convergence. *J. Atmos. Sci.* **43**: 1796–1816.

Rutledge SA, Hobbs PV. 1983. The mesoscale and microscale structure and organization of clouds and precipitation in midlatitude cyclones. Part VIII: A model for the 'seeder-feeder' process in warm-frontal rainbands. *J. Atmos. Sci.* **40**: 1185–1206.

Rutledge SA, Hobbs PV. 1984. The mesoscale and microscale structure and organization of clouds and precipitation in midlatitude cyclones. Part XII: A diagnostic modeling study of precipitation development in narrow cold-frontal rainbands. *J. Atmos. Sci.* **41**: 2949–2972.

Shen X, Wang Y, Li X. 2011. Effects of vertical wind shear and cloud radiatve processes on responses of rainfall to the large-scale forcing during pre-summer heavy rainfall over southern China. *Q. J. R. Meteorol. Soc.* **137**: 236–249.
Soong ST, Ogura Y. 1980. Response of tradewind cumuli to large-scale processes. *J. Atmos. Sci.* **37**: 2035–2050.
Soong ST, Tao WK. 1980. Response of deep tropical cumulus clouds to mesoscale processes. *J. Atmos. Sci.* **37**: 2016–2034.
Sui C-H, Li X, Yang M-J, Huang H-L. 2005. Estimation of oceanic precipitation efficiency in cloud models. *J. Atmos. Sci.* **62**: 4358–4370.
Sui C-H, Li X, Yang M-J. 2007. On the definition of precipitation efficiency. *J. Atmos. Sci.* **64**: 4506–4513.
Tao W-K, Simpson J. 1993. The Goddard Cumulus Ensemble model. Part I: Model description. *Terr. Atmos. Oceanic Sci.* **4**: 35–72.
Tao W-K, Simpson J, McCumber M. 1989. An ice-water saturation adjustment. *Mon. Weather Rev.* **117**: 231–235.
Tao W-K, Johnson D, Shie C-L, Simpson J. 2004. The atmospheric energy budget and large-scale precipitation efficiency of convective systems during TOGA COARE, GATE, SCSMEX, and ARM: Cloud-resolving model simulations. *J. Atmos. Sci.* **61**: 2405–2423.
Wang D, Li X, Tao W-K, Wang Y. 2009. Effects of vertical wind shear on convective development during a landfall of severe tropical storm *Bilis* (2006). *Atmos. Res.* **94**: 270–275.
Weisman ML, Klemp JB. 1982. The dependence of numerically simulated convective storms on vertical wind shear and buoyancy. *Mon. Weather Rev.* **110**: 504–520.
Weller RA, Anderson SP. 1996. Surface meteorology and air-sea fluxes in the western equatorial Pacific warm pool during TOGA COARE. *J. Climate* **9**: 1959–1990.
Zhang MH, Lin JL. 1997. Constrained variational analysis of sounding data based on column-integrated budgets of mass, heat, moisture, and momentum: Approach and application to ARM measurements. *J. Atmos. Sci.* **54**: 1503–1524.

